European Polymer Journal 127 (2020) 109595

Contents lists available at ScienceDirect

European Polymer Journal

journal homepage: www.elsevier.com/locate/europolj

# Anisotropic electromagnetic interference shielding properties of polymer-based composites with magnetically-responsive aligned $Fe_3O_4$ decorated reduced graphene oxide

Sung Yong Hong[a], Ye Chan Kim[b], Mei Wang[c], Jae-Do Nam[a,e], Jonghwan Suhr[a,d,*]

[a] Department of Polymer Science and Engineering, Sungkyunkwan University, 2066, Seoburo, Jangan-gu, Gyeonggi-do, Republic of Korea
[b] Corporate R&D Group, LG Hausys, LG Science Park, 30, Magokjungang 10-to, Gangseo-gu, Seoul, Republic of Korea
[c] State Key Laboratory of Quantum Optics and Quantum Optics Devices, Institute of Laser Spectroscopy, Collaborative Innovation Center of Extreme Optics, Shanxi University, Taiyuan, Shanxi 030006, China
[d] School of Mechanical Engineering, Sungkyunkwan University, 2066, Seoburo, Jangan-gu, Gyeonggi-do, Republic of Korea
[e] Department of Energy Science, Sungkyunkwan University, 2066, Seoburo, Jangan-gu, Gyeonggi-do, Republic of Korea

ARTICLE INFO

*Keywords:*
EMI shielding
Anisotropic properties
$Fe_3O_4$
Graphene oxide
Filler orientation
Magnetic alignment

ABSTRACT

Recently, polymer-based composites for electromagnetic interference (EMI) shielding materials have received considerable attention since the autonomous vehicle market is increasingly growing. However, the strategies for enhancing EMI shielding effectiveness (EMI SE) are limited to the increase of filler loading. Only few studies have been conducted on controlling fillers owing to the technical challenges. In this study, anisotropic EMI shielding properties of polymer-based composites were demonstrated and investigated. In order to control the orientation of reduced graphene oxide (RGO) in thermoplastic polyurethane (TPU), magnetic responsive RGO ($Fe_3O_4$@RGO) was synthesized for filler material. The orientation of $Fe_3O_4$@RGO was controlled in in-plane and out-of-plane direction by applying the magnetic field. For comparison with the aligned $Fe_3O_4$@RGO/TPU composites, random $Fe_3O_4$@RGO/TPU and random RGO/TPU composites were synthesized and characterized. The random $Fe_3O_4$@RGO/TPU composites showed 224% increased EMI SE over random RGO/TPU composites. The highest EMI SE, 250% improvement over random RGO/TPU composite, was observed in in-plane aligned $Fe_3O_4$@RGO composite among the four different composites. This could be attributed to improved electromagnetic wave (EM) loss by introducing magnetic nanoparticles, as well as enlarged effective reflection area of the aligned $Fe_3O_4$@RGO. Our results confirm that the orientation of fillers can play a key role in determining EMI SE in the composites. It can indicate that, if optimized, magnetically-responsive aligned polymer composites could significantly improve EMI SE of the composites by controlling the orientation of fillers, and also be a new solution to create anisotropic composites toward desirable properties.

## 1. Introduction

Recently, electromagnetic pollution has become a serious concern owing to the rapid development of various electronic devices. This is particularly true since the autonomous vehicle market is increasingly growing in our society. This type of pollution usually occurs in the form of electromagnetic interference (EMI) with other electronic devices, which causes malfunction and electromagnetic radiation, and poses potential risks to human health [1,2]. To address the aforementioned issues, novel and high-performance EMI shielding materials have drawn considerable attention in the relevant fields. Polymer-based composites containing electrically conductive nanofillers appear to become more attractive than traditional metal-based EMI shielding materials because of their light weight, applicability, good processability, and corrosion resistance. In particular, polymer-based graphene composites have been extensively investigated as EMI shielding materials due to their high specific surface area and excellent electronic conductivity [3–6].

In polymer-based graphene composites for EMI shielding, high nanofiller loading is required to attain desirable EMI shielding effectiveness (EMI SE). Increasing nanofiller loading in composites would be a simple and easy strategy to enhance the EMI SE of composites. However, it is well-known that higher loadings of nanofillers would

* Corresponding author at: Department of Polymer Science and Engineering & School of Mechanical Engineering, Sungkyunkwan University, 2066, Seoburo, Jangan-gu, Gyeonggi-do, Republic of Korea.
*E-mail address:* suhr@skku.edu (J. Suhr).

https://doi.org/10.1016/j.eurpolymj.2020.109595
Received 13 February 2020; Received in revised form 26 February 2020; Accepted 29 February 2020
Available online 29 February 2020

result in higher costs, poor processability with increasing viscosity, and also poor mechanical properties due to the agglomeration of nanofillers. Thus, a new solution seems to be necessarily developed to overcome the aforementioned issues and further enhance the EMI shielding performance of polymer-based composites. Given that nanofillers such as one-dimensional nanotubes and two-dimensional platelets are geometrically anisotropic, this feature could be effectively utilized to control the nanofillers orientation in polymer materials, which might show great potential to improve and/or engineer material properties including electrical and thermal conductivities [7–11].

However, very few studies have been conducted on the effects of filler orientation because of the technical difficulties in controlling the orientation of fillers in polymer matrix materials. Several approaches have been proposed to attain the well-oriented nanofillers in composites, including electric fields, tape-casting, and freeze-casting followed by sintering and vacuum-assisted filtration, and squeezing process [10–13]. These approaches can yield the platelet-reinforced composites with highly anisotropic properties, but may require multiple processing steps, which would limit the applications only to thin films. Recently, an attractive solution was proposed to control filler orientation or location in a matrix [14] by decorating the reinforcement particle with superparamagnetic nanoparticles (NPs), e.g., iron oxide nanoparticles ($Fe_3O_4$-NPs), to make them magnetically-responsive [14,15]. These coated fillers exhibit an ultrahigh magnetic response that enables remote control over their orientation in low external magnetic fields under low-viscosity suspending fluids. Such fluids can be then consolidated to keep the nanoparticles a preferred magnetically-imposed orientation. This allowed for the creation and development of various microstructures in polymer-based composites [14–16].

Superparamagnetic NPs, which are widely used for various applications in environmental, electronic, and biological processes, were employed to functionalize graphene platelets [17–20]. The functionalization of graphene with superparamagnetic NPs could increase the complex permeability values of graphene because of their large saturation magnetization, thus resulting in a dramatic improvement of the EM wave absorption property [18–21]. Furthermore, the coexistence of graphene and superparamagnetic NP could provide better dispersion in composites, otherwise, they tend to aggregate each other [18,22].

Here, this study investigated the effect of filler orientation on EMI SE of reduced graphene oxide (RGO) reinforced composites. Firstly, magnetically-responsive RGO, i.e., $Fe_3O_4$@RGO, was newly synthesized by introducing iron oxide nanoparticles ($Fe_3O_4$-NPs) on RGO. The orientations of fillers in composites were simply controlled by applying a magnetic field. Thereby, the 250% improvement in EMI shielding effectiveness in in-plane aligned $Fe_3O_4$@RGO composite was demonstrated, compared to randomly dispersed RGO composites. It can indicate that magnetically-responsive aligned polymer composites could not only effectively control the orientation of fillers but also significantly improve EMI SE of the composites. This could provide a new solution to create high performance EMI shielding composite materials.

## 2. Experimental

### 2.1. Materials

Graphene Oxide (GO, GO-V30-100) with greater than 7 μm in lateral size and less than 5 nm in thickness was supplied by Standard Graphene Inc, Ulsan, Korea. Ferrofluid, an aqueous suspension containing 10 wt% of ~10 nm iron oxide nanoparticles ($Fe_3O_4$-NPs) dispersed with a cationic surfactant (EMG-607 Ferrofluid) was obtained from Ferrotec Corporation, Chiba, Japan. Thermoplastic polyurethane (TPU, 60A) was obtained from BASF, Ludwigshafen, Germany. Dimethylformamide (DMF) and hydrazine (35%, $N_2H_4$) were purchased from Merck KGaA, Darmstadt, Germany.

RGO was decorated with superparamagnetic $Fe_3O_4$-NPs to provide magnetic-responsive properties according to a previously reported procedure [14]. The GO suspension (1 mg/ml) was obtained by dispersing 100 mg of GO powder in 100 ml of deionized (DI) water by bath sonication (400 W, 20 Hz) at pH 7. Under continuous and vigorous stirring, 200 $\mu$l of EMG-607 (Ferrofluid) diluted with 5 ml of DI water was added dropwise into the GO suspension to make total weight ratio of $Fe_3O_4$ over GO 10000:2. The suspension was incubated for 2 h to decorate the GO with $Fe_3O_4$-NPs; then, the mixture was further reduced by hydrazine at 90 °C for 6 h. After being cooled to room temperature, the decorated RGO in the solution was washed with distilled water several times. Finally, the decorated RGO was freeze-dried for 25 h to obtain the magnetically-responsive RGO ($Fe_3O_4$@RGO) platelets.

Four different types of TPU composites containing 10 wt% of randomly-oriented RGO, and randomly-oriented $Fe_3O_4$@RGO, and oriented $Fe_3O_4$@RGO in the in-plane, and out-of-plane, respectively were prepared by a solution casting method. Firstly, the desired amount of RGO and $Fe_3O_4$@RGO as reinforcement was dispersed in DMF under bath sonication for 30 min to obtain the $Fe_3O_4$@RGO suspension. Then, the TPU/DMF dilute solution (1 mg/10 ml) was prepared by using magnetic stirring at room temperature for 5 h. The prepared solution was mixed with RGO and $Fe_3O_4$@RGO suspension by vigorously stirring at 60 °C for 24 h. After the mixing process, DMF was carefully removed until the mixture became sufficiently viscous for pouring (~500 mPa.s). However, it was still fluid state so as to align $Fe_3O_4$@RGO fillers under a magnetic field. To align magnetically-responsive $Fe_3O_4$@RGO in TPU, the suspension was placed between two rare-earth magnets that generate a 300 mT magnetic field. For the films with out-of-plane-aligned $Fe_3O_4$@RGO, the magnetic field was applied by using a 20 cm × 10 cm rectangular rare-earth magnets placed over and below the casting mold. For the films with in-plane-aligned $Fe_3O_4$@RGO, the magnetic field was applied with the same magnets placed beside the mold. The molds were heated at 60 °C for 24 h in the fume hood to remove the DMF and consolidate the $Fe_3O_4$@RGO/TPU composites. For the comparison, the composites adding randomly dispersed RGO and $Fe_3O_4$@RGO platelets, respectively were fabricated under the same processing conditions without any external magnetic field.

### 2.2. Material characterization

The electrical charges of $Fe_3O_4$ and GO were evaluated by measuring Zeta potential with Laser Doppler electrophoresis (Malvern Zetasizer Nano ZS, Malvern Inst. Ltd. Malvern, UK).

X-ray diffraction (XRD) analysis was carried out on a XRD diffractometer (Bruker D8 ADVANCE, Bruker AXS, Germany) operated with Cu Kα radiation at a generator current of 40 mA and voltage of 40 kV. X-ray photoelectron spectroscopy (XPS) was performed with a XPS spectrometer (Thermo ESCALAB250, Thermo-VG Scientific, USA) using Al (mono) Kα radiation to analyze the surface chemistry of $Fe_3O_4$@RGO. Raman spectra were recorded by using a Raman Station (Bruker FRA 160/S, Bruker AXS, Germany) with a 633 nm laser source.

The saturation magnetization and coercivity of the samples were measured by using a vibration-sample magnetometer (VSM, Lakeshore 7400, Chicago, IL, USA) at a maximum applied field of 10 kOe.

Transmission electron microscopy (TEM, Tecnai G2 F30 S-Twin, S-TWIN, USA) was used to characterize the morphology of $Fe_3O_4$@RGO at an accelerating voltage of 200 kV. The structural morphology of $Fe_3O_4$@RGO/TPU composite surface was also observed using a scanning electron microscopy (SEM, JEOL JSM-7401F, Tokyo, Japan).

The EMI shielding performance was measured with a vector network analyzer (VNA, Keysight E8364A, Agilent, CA, USA) at room temperature in the X-band (8–12 GHz). The toroidal samples of 1.0 mm in thickness ($\psi_{out}$: 7.00 mm, $\psi_{in}$: 3.04 mm) were placed inside the 7/3 mm coaxial airline between the inner and outer conductors; the samples' plane was perpendicular to the coaxial line axis. The total EMI SE ($SE_T$) is equal to the summation of EMI SE reflection ($SE_R$) and EMI SE absorption ($SE_A$) (Eq. (5), while EMI SE reflection (Eq. (3)), were

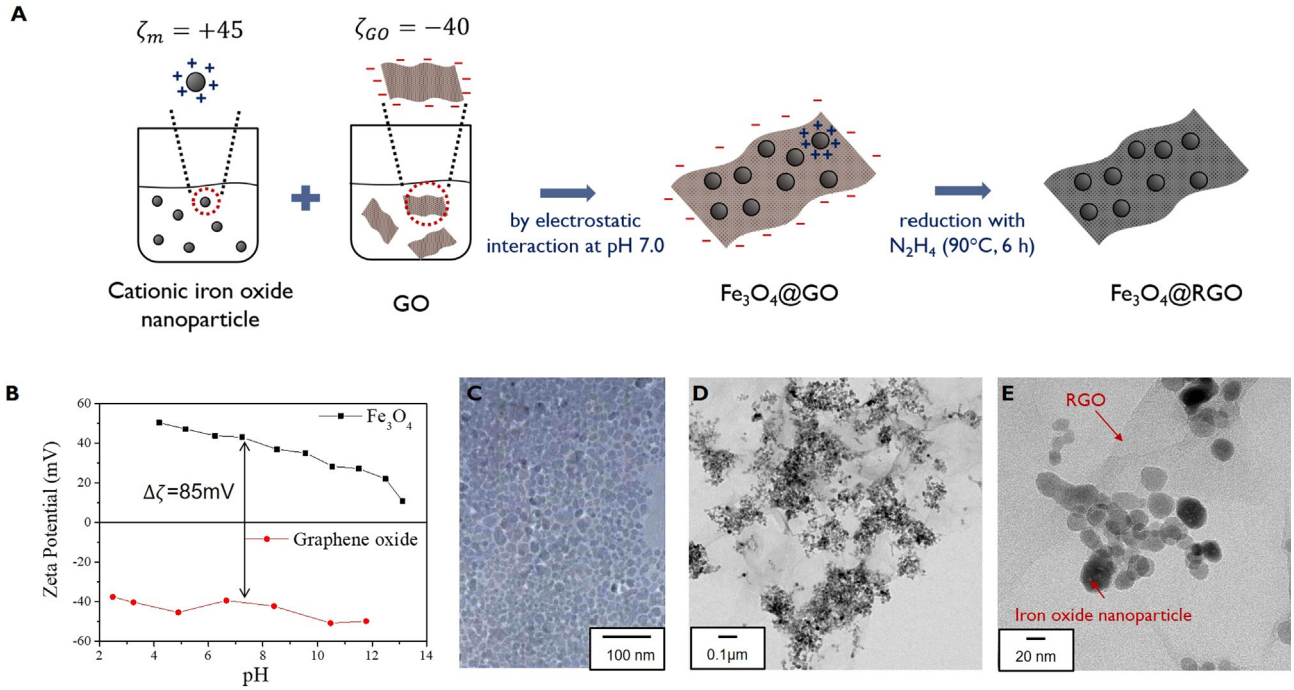


**Fig. 1.** Schematic for the preparation of $Fe_3O_4$@RGO through electrostatic adsorption between $Fe_3O_4$-NPs and GO and in-situ reduction of $Fe_3O_4$@GO (A), Zeta potential of negatively-charged GO and positively-charged $Fe_3O_4$-NPs as a function of pH (B); and TEM images of $Fe_3O_4$ provided from the manufacturer (C) [23] and synthesized $Fe_3O_4$@RGO (D and E).

determined based on the measured S parameters (Eq. (1)). S parameters for EMI SE absorption can be obtained by subtracting $S_{11}$ and $S_{21}$ from 1 (Eqs. (2) and (4)).

$$R = |S_{11}|^2 \quad T = |S_{21}|^2, \tag{1}$$

$$A = 1 - R - T \tag{2}$$

$$SE_R = -10log(1 - R) \tag{3}$$

$$SE_A = -10log\left(\frac{T}{1 - R}\right) \tag{4}$$

$$SE_T = SE_R + SE_A \tag{5}$$

## 3. Results and discussion

Magnetically-responsive $Fe_3O_4$@RGO was synthesized by electrostatic adsorption between $Fe_3O_4$ and GO, and followed by in-situ chemical reduction of $Fe_3O_4$@GO. The schematic illustration for the preparation of magnetic-responsive $Fe_3O_4$ decorated RGO is shown in Fig. 1A. The adsorption of $Fe_3O_4$ on GO was driven by electrostatic attraction. The electrostatic charge of each material was characterized with Zeta potential measurement. The Zeta potential of cationic $Fe_3O_4$-NPs at pH 7.0 showed a positive charge (~+45 mV), while the GO sheets exhibited a negative charge (~-40 mV) (Fig. 1B). The large difference between the negative and positive charges of each material ($\Delta\zeta$ = 85 mV) resulted in strong electrostatic adsorption of $Fe_3O_4$ on GO platelets. It could be also expected that the electrostatic interaction driven adsorption may be further promoted by short-range van der Waals attractions, which would then lead to becoming irreversible for a sufficient time [14]. After the electrostatic adsorption, the chemical reduction of $Fe_3O_4$@GO was conducted to increase the electrical conductivity of the synthesized platelets, which results in generation of $Fe_3O_4$@RGO. The successful attachment of $Fe_3O_4$ onto RGO sheets was confirmed by TEM characterization (Fig. 1C, 1D and 1E). The TEM image of $Fe_3O_4$-NPs with the average nominal particle diameter of ~10 nm is displayed in Fig. 1C [23]. The Fig. 1D and 1E can indicate that the $Fe_3O_4$-NPs are shown to be fairly well bonded to the RGO sheets.

The structures of GO and $Fe_3O_4$@RGO were analyzed with XRD measurement (Fig. 2A). Typical XRD patterns of GO (0 0 1) at $2\theta$ = 10.6° appeared (black line in Fig. 2A). The characteristic diffraction peaks of $Fe_3O_4$-NPs are presented in $Fe_3O_4$@RGO (red line in Fig. 2A), which can be assigned to (1 1 1), (2 2 0), (3 1 1), (4 0 0), (4 2 2), (5 1 1), (4 4 0), and (5 3 3) according to the Joint Committee on Powder Diffraction Standard No. 19-0629 [24].

Raman spectroscopy was used to confirm the structural changes during the reduction process from $Fe_3O_4$@GO to $Fe_3O_4$@RGO. As shown in Fig. 2B, compared with GO (black line), the G-band of graphene in $Fe_3O_4$@RGO (red line) shifted from 1569 to 1588 $cm^{-1}$, which is pretty close to that of pristine graphite (1579 $cm^{-1}$), indicating the successful reduction of GO.

XPS was used to further analyze the chemical compositions and functional groups of GO and $Fe_3O_4$@RGO (Fig. 2C–E) [25–27]. The C1s spectra seen in Fig. 2C can be deconvoluted into four types of functional groups: non-oxygenated C—C bond at 284.6 eV; C—O bond at 286.5 eV; C═O bond at 287.8 eV; and O—C═O bond at 289.3 eV, indicating that GO would have enough oxygen functional groups [25–27]. In contrast, in the C1s spectra of $Fe_3O_4$@RGO (Fig. 2D), the relative intensities of the three components related to the functional group (C—O, C═O, and O—C═O) are found to be significantly decreased, indicating the effective deoxygenation of GO during the reduction process. The Fe 2p spectrum (Fig. 2E) can be deconvoluted into two peaks at 713 and 726 eV, corresponding to Fe $2p_{3/2}$ and Fe $2p_{1/2}$ of $Fe_3O_4$, respectively, which can be an indicator of the attachment of the iron oxide nanoparticles ($Fe_3O_4$-NPs) onto the RGO surface.

VSM results show the magnetic responses of $Fe_3O_4$@RGO in Fig. 2F. The magnetization curves of $Fe_3O_4$@RGO were measured at room temperature under the magnetic fields ranging from −10 to 10 kOe. The magnetic hysteresis loop of $Fe_3O_4$@RGO was observed to be a typical superparamagnetic behavior, i.e., S-like shape and reversible behavior with nearly zero coercivity (Fig. 2F). Superparamagnetism could disperse $Fe_3O_4$@RGO in the solution with negligible magnetic

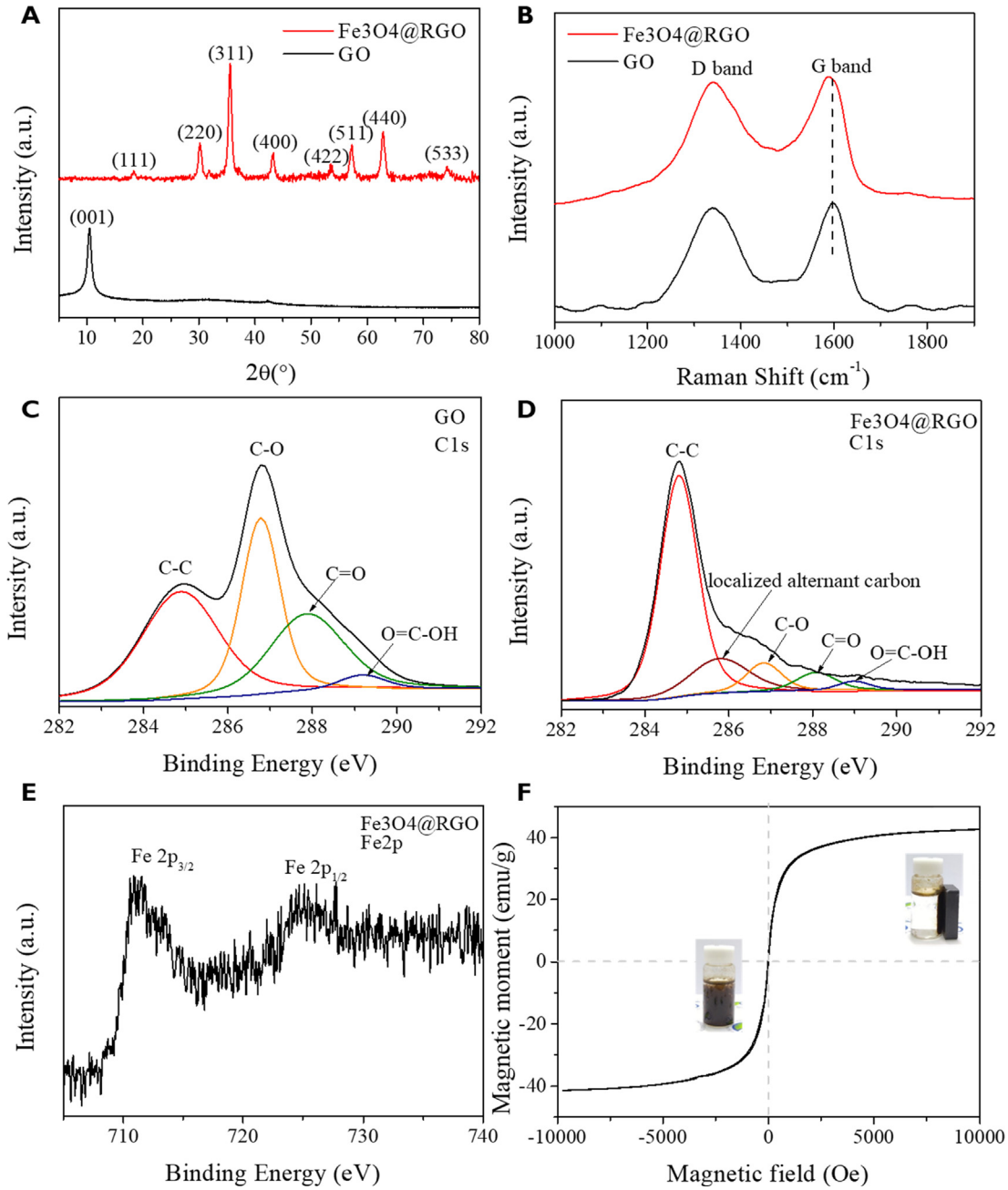


**Fig. 2.** XRD patterns of GO and $Fe_3O_4$@RGO (A), Raman spectra of GO and $Fe_3O_4$@RGO with a 633 nm laser (B), C 1s XPS spectra of GO (C), C 1s XPS spectra of $Fe_3O_4$@RGO (D), Fe 2p XPS spectra of $Fe_3O_4$@RGO (E), magnetization hysteresis loops of $Fe_3O_4$@RGO at room temperature. The insets show photographs of $Fe_3O_4$@RGO in water and their response to an external magnetic field (F).

interactions between the RGOs preventing clustering and restacking [28]. The susceptive magnetic response of $Fe_3O_4$@RGO is shown in Fig. 2F. The left inset shows a digital photograph of $Fe_3O_4$@RGO dispersion in DI water. The right inset presents the facile separation of $Fe_3O_4$@RGO in DI water under an external magnetic field.

Magnetically-responsive aligned $Fe_3O_4$@RGO/TPU composites were successfully prepared by simply applying magnetic fields. For comparison, randomly-oriented $Fe_3O_4$@RGO/TPU composites were also fabricated without any magnetic field. Fig. 3A shows a schematic illustration of the microstructure of the randomly-oriented $Fe_3O_{4@}$RGO/TPU composite. The random orientation and distribution of $Fe_3O_4$@RGO in the composites were confirmed by SEM characterization (Fig. 3B). Fig. 3C and 3E show the aligned $Fe_3O_4$@RGO/TPU composites fabricated by applying the linear and uniform magnetic fields generated with the rare-earth magnets, respectively. In the top-view and side-view SEM images of the in-plane aligned $Fe_3O_4$@RGO/TPU composite (Fig. 3C and 3E), it can show the magnetic-field induced orientation of $Fe_3O_4$@RGO in the composites. However, unfortunately, $Fe_3O_4$@RGOs are not perfectly parallel to in-plane direction, because of the loop-shaped three-dimensional magnetic field. Similar morphologies were found in previous studies [14,16].

The EMI SE of RGO/TPU and $Fe_3O_4$@RGO/TPU composites with different filler orientations was measured in the EM frequency range 8–12 GHz (X-band). All the composites exhibited weak frequency-dependent EMI SE in the measured EM range (Fig. 4A). The 224% increase of EMI SE in random $Fe_3O_4$@RGO/TPU composite compared to random RGO/TPU composite was confirmed in the X-band. The random $Fe_3O_4$@RGO/TPU composite exhibited ~15.51±1.6 dB, while random

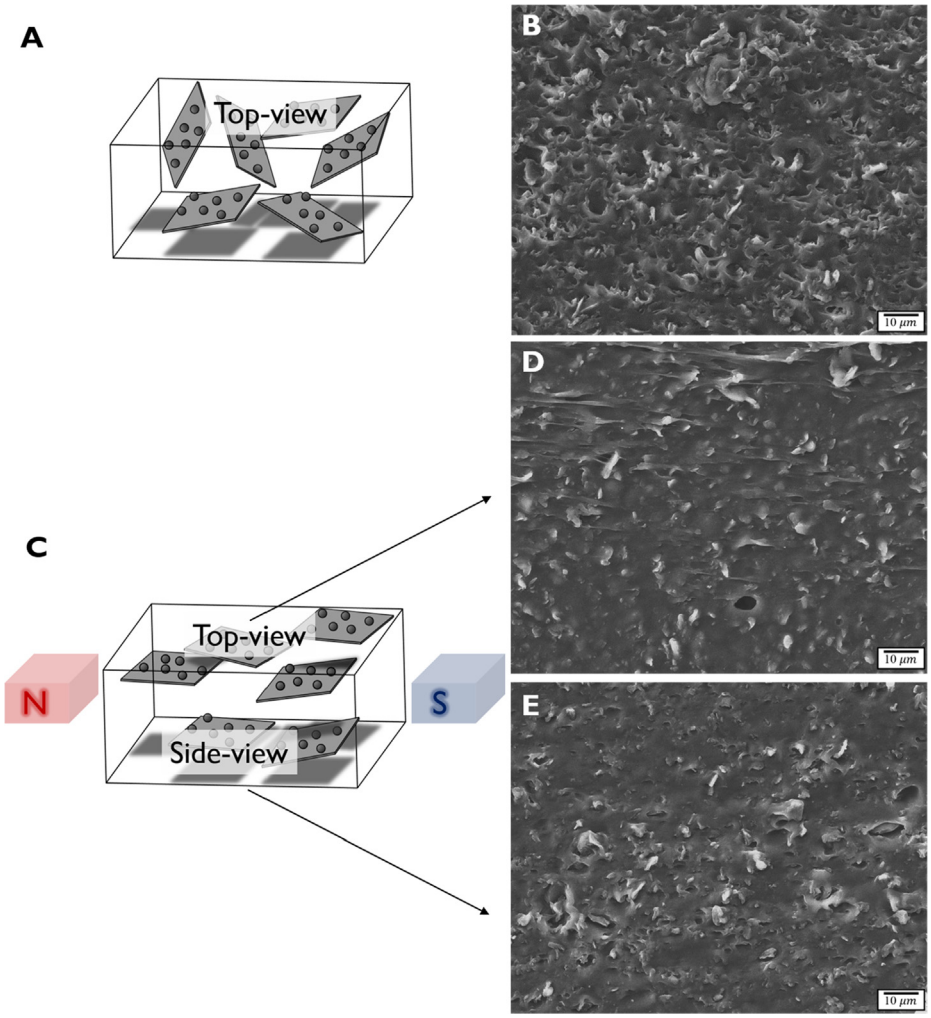


**Fig. 3.** Schematic and SEM images of $Fe_3O_4$@RGO/TPU composites; (A and B) randomly-oriented, top-view (C and D), and side-view (C and E) of magnetic-field-induced alignment of $Fe_3O_4$@RGO.

RGO/TPU composite displayed ~6.90±1.00 dB. The enhanced EMI SE is believed to be attributed to the increase in EM absorption loss ($SE_A$) by the incorporation of $Fe_3O_4$–NPs on RGO platelets. The random $Fe_3O_4$@RGO/TPU composite exhibited ~12.6 ~ 4.71 ±1.5 9 dB of EMI $SE_A$, while the random RGO/TPU composite ~4.71 ±1.00 (Fig. 4B). The enhanced $SE_A$ of $Fe_3O_4$@RGO/TPU composites in this study was believed to be contributed from two key properties: the magnetic loss of incorporated $Fe_3O_4$-NPs and the enhanced dielectric loss due to the interfacial polarization between the $Fe_3O_4$-NPs and RGO [20,29–31]. As previously reported by J.J. Guo et al. [29], interfacial polarization can be developed between $Fe_3O_4$-NPs and RGO, and also between neighboring $Fe_3O_4$-NPs.

The effects of the magnetically-responsive alignment were also shown in Fig. 4A. The in-plane-aligned $Fe_3O_4$@RGO composite exhibits the highest EMI SE of ~17.22 ±1.8 dB, while random $Fe_3O_4$@RGO/TPU composites and out-of-plane aligned $Fe_3O_4$@RGO/TPU composite display ~15.51 ±1.6 dB and ~13.93 ±1.5 dB in X-band, respectively. These results are mainly attributed to $Fe_3O_4$@RGO orientation and the corresponding EM attenuation by reflection and internal multiple reflection degree of composite. It is reported that in particulate composites, the EM reflection and the internal multiple reflections are highly dependent on the effective reflection area of fillers [32].

The effective reflection area in this study can be defined as the summation of the projection area of $Fe_3O_4$@RGO on the against nominal incident wave (Eq. (6)).

$$A_{eff} = \sum_{i=1}^{n} A_i cos\theta_i \tag{6}$$

where $\theta_i$ is the angle for each $Fe_3O_4$@RGO filler to the tangent plane of the incident wave, and $A_i$ is the area for each $Fe_3O_4$@RGO filler. It is apparent that the in-plane aligned $Fe_3O_4$@RGO composite obtains the largest effective area, while the effective area of out-of-plane aligned $Fe_3O_4$@RGO composite would be much smaller than random $Fe_3O_4$@RGO composite owing to the high aspect ratio of RGO with a two-dimensional sheet shape.

The large effective reflection area of in-plane aligned $Fe_3O_4$@RGO fillers is expected to contribute to greater EMI $SE_A$ by multiple internal reflections [33–36], which result from repeated reflections as various interfaces or surfaces on the shielding material in particulate composites as well. The incident EM waves entering the composites could be repeatedly reflected and scattered between these interfaces, and ultimately dissipated as heat [37,38]. It is considered that compared to out-of-plane aligned $Fe_3O_4$@RGO fillers and random $Fe_3O_4$@RGO fillers, the in-plane aligned $Fe_3O_4$@RGO fillers have a higher probability of repeated reflection and scattering of incident waves between $Fe_3O_4$@RGO fillers owing to the larger effective area as illustrated in Fig. 4C and B. Accordingly, random $Fe_3O_4$@RGOcomposite showed greater EMI $SE_R$ and $SE_A$ than the out-of-plane aligned $Fe_3O_4$@RGO composite, because of their relatively larger effective area.

It is noted here that the EMI SE of in-plane aligned $Fe_3O_4$@RGO composite presents 250% higher value (~17.22 ±1.8 dB) compared to random RGO/TPU composite (~6.90 ±1.00 dB) in X-band. The poor

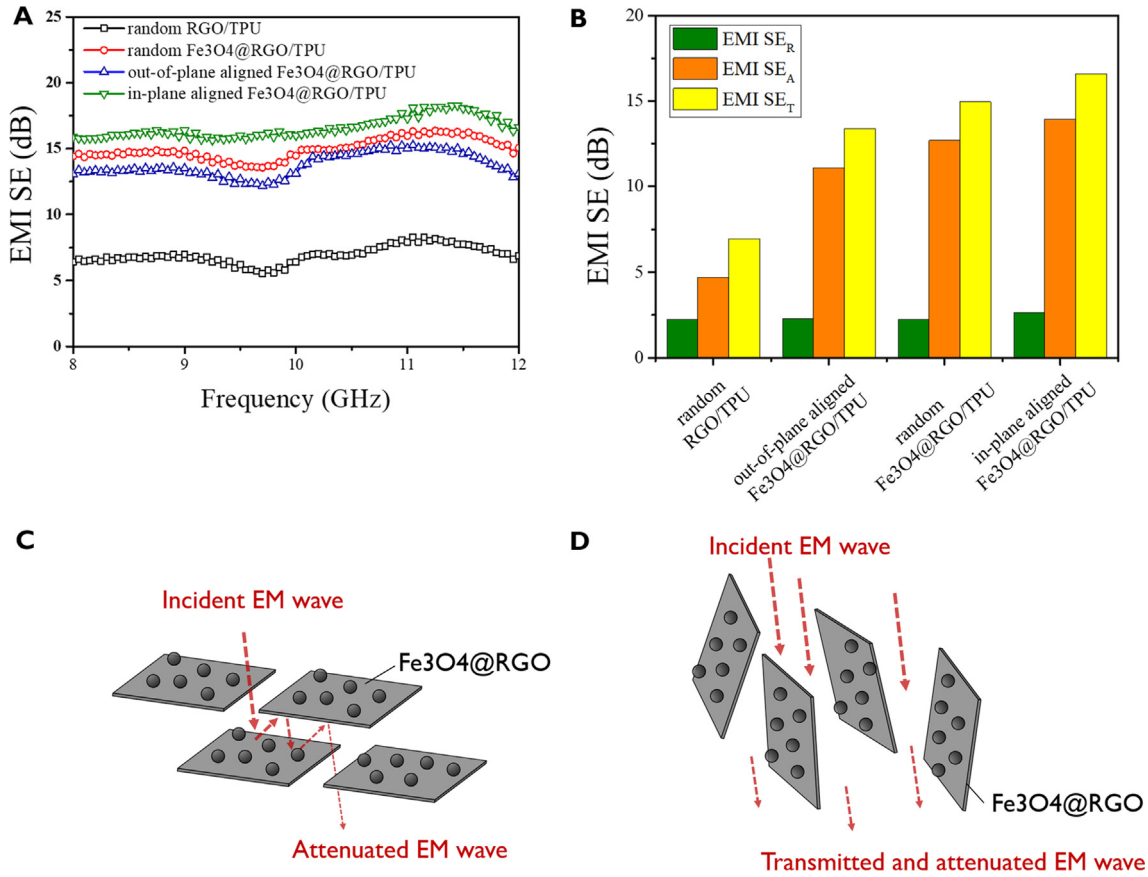


**Fig. 4.** EMI shielding effectiveness results as a function of frequency measured in the 8–12 GHz range (X-band) of the RGO/TPU and $Fe_3O_4$@RGO/TPU composites with three different $Fe_3O_4$@RGO orientations: random, out-of-plane, and in-plane (A). Total EMI SE ($SE_T$) of the RGO/TPU and three different $Fe_3O_4$@RGO/TPU, and their EMI SE reflection ($SE_R$) and EMI absorption ($SE_A$) (B). EMI SE Schematic description of EMI shielding mechanism of $Fe_3O_4$@RGO aligned TPU; in-plane direction (C) and out-of-plane direction (D).

EMI SE of random RGO/TPU composite seems to result from coupled low EM reflection from small effective reflection area with low EM absorption from the absence of $Fe_3O_4$-NPs.

## 4. Conclusions

The highly anisotropic EMI SE of RGO particulate composites was demonstrated by controlling the filler orientation under magnetic fields. To introduce magnetically-responsive features into RGO, GO was decorated with $Fe_3O_4$-NPs by electrostatic adsorption with in-situ reduction process. The observed 250% improvement in EMI SE of in-plane aligned $Fe_3O_4$@RGO/TPU composites over random RGO/TPU composites, is attributed to not only enlarged effective reflection area from well-oriented $Fe_3O_4$@RGO, but also $Fe_3O_4$@-NPs incorporation induced EM magnetic loss and dielectric loss from interface polarization between $Fe_3O_4$@-NPs and RGO.

Our test results can indicate that the orientation of fillers in the polymer matrix can play a critical role in determining EMI SE in the composites. In addition, this study shows the great promise in developing polymer composites with high EMI SE with only a minimal amount of filler addition by exploiting the high aspect ratio of nano-sized filler materials such as carbon nanotubes or graphene. This could provide a new material solution in a variety of engineering applications including mobile devices, vehicle and aircraft electronics, and medical devices that may require EMI protection.

## CRediT authorship contribution statement

**Sung Yong Hong:** Investigation, Writing - original draft, Writing - review & editing. **Ye Chan Kim:** Methodology, Investigation. **Mei Wang:** Resources. **Jae-Do Nam:** Resources. **Jonghwan Suhr:** Funding acquisition, Project administration, Supervision.

## Declaration of Competing Interest

The authors declare that they have no known competing financial interests or personal relationships that could have appeared to influence the work reported in this paper.

## Acknowledgments

This work was supported by the National Research Foundation of Korea (NRF) grant funded by the Korea government (MSIP) (2018R1A2B2001565).

## References

[1] B. Shen, W. Zhai, W. Zheng, Ultrathin flexible graphene film: an excellent thermal conducting material with efficient EMI shielding, Adv. Funct. Mater. 24 (28) (2014) 4542–4548.
[2] D. Chung, Electromagnetic interference shielding effectiveness of carbon materials, Carbon 39 (2) (2001) 279–285.
[3] J. Liang, Y. Wang, Y. Huang, Y. Ma, Z. Liu, J. Cai, C. Zhang, H. Gao, Y. Chen, Electromagnetic interference shielding of graphene/epoxy composites, Carbon 47 (3) (2009) 922–925.
[4] H.-B. Zhang, Q. Yan, W.-G. Zheng, Z. He, Z.-Z. Yu, Tough graphene− polymer microcellular foams for electromagnetic interference shielding, ACS Appl. Mater. Interfaces 3 (3) (2011) 918–924.
[5] G. Lovat, Equivalent circuit for electromagnetic interaction and transmission through graphene sheets, IEEE Trans. Electromagn. Compat. 54 (1) (2012) 101–109.

[6] S.K. Hong, K.Y. Kim, T.Y. Kim, J.H. Kim, S.W. Park, J.H. Kim, B.J. Cho, Electromagnetic interference shielding effectiveness of monolayer graphene, Nanotechnology 23 (45) (2012) 455704.
[7] W. Guo, C. Liu, X. Sun, Z. Yang, H.G. Kia, H. Peng, Aligned carbon nanotube/polymer composite fibers with improved mechanical strength and electrical conductivity, J. Mater. Chem. 22 (3) (2012) 903–908.
[8] H. Huang, C. Liu, Y. Wu, S. Fan, Aligned carbon nanotube composite films for thermal management, Adv. Mater. 17 (13) (2005) 1652–1656.
[9] T. Terao, C. Zhi, Y. Bando, M. Mitome, C. Tang, D. Golberg, Alignment of boron nitride nanotubes in polymeric composite films for thermal conductivity improvement, J. Phys. Chem. C 114 (10) (2010) 4340–4344.
[10] R. Libanori, F.H. Münch, D.M. Montenegro, A.R. Studart, Hierarchical reinforcement of polyurethane-based composites with inorganic micro-and nanoplatelets, Compos. Sci. Technol. 72 (3) (2012) 435–445.
[11] E. Munch, M.E. Launey, D.H. Alsem, E. Saiz, A.P. Tomsia, R.O. Ritchie, Tough, bio-inspired hybrid materials, Science 322 (5907) (2008) 1516–1520.
[12] T.-H. Lin, W.-H. Huang, I.-K. Jun, P. Jiang, Bioinspired assembly of surface-roughened nanoplatelets, J. Colloid Interface Sci. 344 (2) (2010) 272–278.
[13] T.L. Li, S.L.C. Hsu, Preparation and properties of thermally conductive photosensitive polyimide/boron nitride nanocomposites, J. Appl. Polym. Sci. 121 (2) (2011) 916–922.
[14] R.M. Erb, R. Libanori, N. Rothfuchs, A.R. Studart, Composites reinforced in three dimensions by using low magnetic fields, Science 335 (6065) (2012) 199–204.
[15] H. Yan, Y. Tang, W. Long, Y. Li, Enhanced thermal conductivity in polymer composites with aligned graphene nanosheets, J. Mater. Sci. 49 (15) (2014) 5256–5264.
[16] Z. Lin, Y. Liu, S. Raghavan, K.-S. Moon, S.K. Sitaraman, C.-P. Wong, Magnetic alignment of hexagonal boron nitride platelets in polymer matrix: toward high performance anisotropic polymer composites for electronic encapsulation, ACS Appl. Mater. Interfaces 5 (15) (2013) 7633–7640.
[17] V. Chandra, J. Park, Y. Chun, J.W. Lee, I.-C. Hwang, K.S. Kim, Water-dispersible magnetite-reduced graphene oxide composites for arsenic removal, ACS Nano 4 (7) (2010) 3979–3986.
[18] H. He, C. Gao, Supraparamagnetic, conductive, and processable multifunctional graphene nanosheets coated with high-density $Fe_3O_4$ nanoparticles, ACS Appl. Mater. Interfaces 2 (11) (2010) 3201–3210.
[19] T. Wang, Z. Liu, M. Lu, B. Wen, Q. Ouyang, Y. Chen, C. Zhu, P. Gao, C. Li, M. Cao, Graphene–$Fe_3O_4$ nanohybrids: synthesis and excellent electromagnetic absorption properties, J. Appl. Phys. 113 (2) (2013) 024314.
[20] X. Sun, J. He, G. Li, J. Tang, T. Wang, Y. Guo, H. Xue, Laminated magnetic graphene with enhanced electromagnetic wave absorption properties, J. Mater. Chem. C 1 (4) (2013) 765–777.
[21] G. Sun, B. Dong, M. Cao, B. Wei, C. Hu, Hierarchical dendrite-like magnetic materials of $Fe_3O_4$, $\gamma$-$Fe_2O_3$, and Fe with high performance of microwave absorption, Chem. Mater. 23 (6) (2011) 1587–1593.
[22] X. Huo, J. Liu, B. Wang, H. Zhang, Z. Yang, X. She, P. Xi, A one-step method to produce graphene–$Fe_3O_4$ composites and their excellent catalytic activities for three-component coupling of aldehyde, alkyne and amine, J. Mater. Chem. A 1 (3) (2013) 651–656.
[23] FerroTec, EMG 607, Water based ferrofluid with cationic surfactant coated magnetic-nano particle, Ferrotec.
[24] J. Wan, W. Cai, J. Feng, X. Meng, E. Liu, In situ decoration of carbon nanotubes with nearly monodisperse magnetite nanoparticles in liquid polyols, J. Mater. Chem. 17 (12) (2007) 1188–1192.
[25] H.-B. Zhang, J.-W. Wang, Q. Yan, W.-G. Zheng, C. Chen, Z.-Z. Yu, Vacuum-assisted synthesis of graphene from thermal exfoliation and reduction of graphite oxide, J. Mater. Chem. 21 (14) (2011) 5392–5397.
[26] Y. Cong, M. Long, Z. Cui, X. Li, Z. Dong, G. Yuan, J. Zhang, Anchoring a uniform $TiO_2$ layer on graphene oxide sheets as an efficient visible light photocatalyst, Appl. Surf. Sci. 282 (2013) 400–407.
[27] Y.-C. Shi, J.-J. Feng, X.-X. Lin, L. Zhang, J. Yuan, Q.-L. Zhang, A.-J. Wang, One-step hydrothermal synthesis of three-dimensional nitrogen-doped reduced graphene oxide hydrogels anchored PtPd alloyed nanoparticles for ethylene glycol oxidation and hydrogen evolution reactions, Electrochim. Acta 293 (2019) 504–513.
[28] X. Fan, G. Jiao, W. Zhao, P. Jin, X. Li, Magnetic Fe 3 O 4–graphene composites as targeted drug nanocarriers for pH-activated release, Nanoscale 5 (3) (2013) 1143–1152.
[29] P. Guan, X. Zhang, J. Guo, Assembled Fe3O4 nanoparticles on graphene for enhanced electromagnetic wave losses, Appl. Phys. Lett. 101 (15) (2012) 153108.
[30] K. Singh, A. Ohlan, V.H. Pham, R. Balasubramaniyan, S. Varshney, J. Jang, S.H. Hur, W.M. Choi, M. Kumar, S. Dhawan, Nanostructured graphene/$Fe_3O_4$ incorporated polyaniline as a high performance shield against electromagnetic pollution, Nanoscale 5 (6) (2013) 2411–2420.
[31] B. Shen, W. Zhai, M. Tao, J. Ling, W. Zheng, Lightweight, multifunctional polyetherimide/graphene@ $Fe_3O_4$ composite foams for shielding of electromagnetic pollution, ACS Appl. Mater. Interfaces 5 (21) (2013) 11383–11391.
[32] W.-L. Song, M.-S. Cao, M.-M. Lu, J. Yang, H.-F. Ju, Z.-L. Hou, J. Liu, J. Yuan, L.-Z. Fan, Alignment of graphene sheets in wax composites for electromagnetic interference shielding improvement, Nanotechnology 24 (11) (2013) 115708.
[33] W.-L. Song, X.-T. Guan, L.-Z. Fan, W.-Q. Cao, C.-Y. Wang, Q.-L. Zhao, M.-S. Cao, Magnetic and conductive graphene papers toward thin layers of effective electromagnetic shielding, J. Mater. Chem. A 3 (5) (2015) 2097–2107.
[34] B. Shen, W. Zhai, M. Tao, J. Ling, W. Zheng, Lightweight, multifunctional polyetherimide/graphene@$Fe_3O_4$ composite foams for shielding of electromagnetic pollution, ACS Appl. Mater. Interfaces 5 (21) (2013) 11383–11391.
[35] D.X. Yan, H. Pang, B. Li, R. Vajtai, L. Xu, P.G. Ren, J.H. Wang, Z.M. Li, Structured reduced graphene oxide/polymer composites for ultra-efficient electromagnetic interference shielding, Adv. Funct. Mater. 25 (4) (2015) 559–566.
[36] B. Shen, Y. Li, W. Zhai, W. Zheng, Compressible graphene-coated polymer foams with ultralow density for adjustable electromagnetic interference (EMI) shielding, ACS Appl. Mater. Interfaces 8 (12) (2016) 8050–8057.
[37] C. Liu, S. Ye, J. Feng, The preparation of compressible and fire-resistant sponge-supported reduced graphene oxide aerogel for electromagnetic interference shielding, Chem.–Asian J. 11 (18) (2016) 2586–2593.
[38] T. McNally, P. Pötschke, Polymer-carbon nanotube composites: Preparation, properties and applications, Elsevier, 2011.